ELSEVIER

Journal of Structural Geology 25 (2003) 2005–2021

JOURNAL OF STRUCTURAL GEOLOGY

www.elsevier.com/locate/jsg

Analogue modelling of the influence of shape and particle/matrix interface lubrication on the rotational behaviour of rigid particles in simple shear

Stefano Ceriani[a,*], Neil S. Mancktelow[b], Giorgio Pennacchioni[c]

[a]*Geologisch-Palaeontologisches Institut, Bernoullistr. 32, 4056 Basel, Switzerland*
[b]*Geologisches Institut, ETH-Zentrum, CH-8092 Zürich, Switzerland*
[c]*Dipartimento di Geologia, Paleontologia e Geofisica, Università di Padova, Via Giotto 1, 35137 Padova, Italy*

Received 18 September 2002; received in revised form 28 February 2003; accepted 7 March 2003

Abstract

The rotational behaviour of a rigid particle embedded in a linear viscous matrix undergoing cylindrical simple shear (Couette) flow was studied in 2D rock-analogue experiments. The influence of particle shape (elliptical vs. monoclinic), aspect ratio and the nature of the matrix/particle interface (lubricated vs. unlubricated) was investigated. Both matrix (PDMS) and lubricant (liquid soap) were linear viscous, with a viscosity ratio of ca. 10^4. Without lubricant, the rotational behaviour of all particles closely approximates the Jeffery theory. Lubricated monoclinic particles with the long diagonal initially parallel to the shear direction show back rotation and approach a stable position. Lubricated elliptical particles initially parallel to the shear direction also show back rotation but only transiently stabilize. Weak planar zones in the matrix adjacent to unlubricated elliptical particles do not induce backward rotation. In general for elliptical particles, rotation rate as a function of orientation depends on axial ratio and thickness of the lubricant mantle. For thick mantles (initially $>10\%$ of the volume of the particle), rotation rates are faster than Jeffery theory. For very thin mantles they are markedly slower compared with thick mantles, particularly when the long axis is nearly parallel to the shear direction. Rotation rates are never strictly zero, so true stabilization does not occur. However, for more elongate particles (axial ratio $= 6$) rotation rates are so slow that a very strong shape preferred orientation would develop in a lubricated elliptical particle population. In experiments, the volume of lubricant is constant and the thickness adjacent to the long side of the particle progressively decreases with increasing strain. In natural examples of porphyroclast systems, the weak mantle continually develops by recrystallization and/or cataclasis of the rigid clast core and a steady state between production and thinning could be attained, potentially leading to true stabilization for particles with a high axial ratio.

Keywords: Analogue modelling; Rigid particles; Porphyroclasts; Rotation; Stabilization; Shear zones

1. Introduction

Porphyroclast systems in highly strained rocks are often used as sense of shear indicators (Simpson and Schmid, 1983; Passchier and Simpson, 1986) and have been applied, in some cases, to estimate the kinematics of flow (Passchier, 1987). The use of the shape preferred orientation (SPO) of porphyroclasts as a vorticity gauge in natural mylonites is based on the Jeffery (1922) theory (Passchier, 1987; Masuda et al., 1995), which assumes that: (i) particles are rigid ellipsoids; (ii) the particle–matrix interface is coherent; and (iii) the matrix has a Newtonian rheology. However, as recent studies have emphasized (Pennacchioni et al., 2001; Mancktelow et al., 2002; ten Grotenhuis et al., 2002a), mylonites often contain rigid porphyroclasts whose SPO cannot be explained by the Jeffery theory. These porphyroclasts have a strong SPO with the particle long axis oriented at a small antithetic angle to the shear plane (e.g. typical sigma porphyroclast systems and 'mica-fish'). The mechanism producing this SPO is still not unequivocally established but it has been demonstrated in analogue experiments that interface slip could be an important factor (Ildefonse and Mancktelow, 1993; ten Brink and Passchier, 1995; Stewart, 1997; Marques and Coelho, 2001; Mancktelow et al., 2002). From microstructural observations, interface slip has also been proposed as a possible mechanism for stabilization of natural rigid porphyroclasts

* Corresponding author. Tel.: +41-61-267-35-95; fax: +41-61-267-36-13.
E-mail address: stefano.ceriani@unibas.ch (S. Ceriani).

0191-8141/03/$ - see front matter © 2003 Elsevier Ltd. All rights reserved.
doi:10.1016/S0191-8141(03)00098-1

(Pennacchioni et al., 2001) and mica fish (Lister and Snoke, 1984).

As shown by previous analogue-modelling studies (Ghosh and Ramberg, 1976; Arbaret et al., 2001), the behaviour of rigid particles of different shapes embedded in a Newtonian matrix undergoing simple shear is not significantly different from that predicted for an enveloping ellipse by the analytical solution of Jeffery (1922). Ferguson (1979) argued that this solution could also be extended to non-Newtonian materials and Arbaret et al. (2001) demonstrated that the 2D analysis is also a reasonable approximation for the behaviour of 3D objects in simple shear (Hinch and Leal, 1979; Freeman, 1985; Ježek, 1994; Ježek et al., 1994).

Strong deviation in the kinematic behaviour of particles with respect to the analytical solution of Jeffery's equation (1922) has, however, been observed in other analogue experiments. This has been attributed to several factors. Lack of bonding between particle and matrix or the presence of a thin weak layer around an elliptical particle can markedly reduce the rotation rate when the long axis of the particle is close to the shear direction (Ildefonse and Mancktelow, 1993; ten Brink and Passchier, 1995; Mancktelow et al., 2002). The presence of a weak layer can also lead to the stabilization of an elliptical particle in narrow shear zones, where the width of the shear zone is less than the longest dimension of the particle (Marques and Coelho, 2001). An enveloping weak layer can even induce back (antithetic) rotation in certain orientations (Marques and Coelho, 2001; Mancktelow et al., 2002). In the case of monoclinic particles with straight sides (which approximate the shape of many 'mica fish' in natural mylonites, see e.g. Passchier and Trouw, 1996, fig. 5.27), the presence of a weak layer can lead to stabilization of the particle, with the straight side near parallel or at a small angle to the shear plane (Mancktelow et al., 2002). For particles exceeding a critical aspect ratio, stabilization and antithetic rotation in certain orientations can also be caused in theory by a component of pure shear (Ghosh and Ramberg, 1976), but the consequent dependence of the stable orientation of the particle on its aspect ratio is not observed in natural SPOs (Pennacchioni et al., 2001). Small-scale shear strain localization in the matrix has also been proposed as a mechanism for stabilization of monoclinic rigid particles, on the basis of experiments with cohesionless granular material showing Mohr–Coulomb behaviour (ten Grotenhuis et al., 2002a).

The current study uses analogue scale models to systematically analyse the two-dimensional behaviour of rigid particles in a Newtonian viscous matrix. Specifically, the influence of a lubricating layer at the particle boundary and its thickness is investigated for different initial particle orientations. Consistent with the common shapes of porphyroclasts in mylonites, both elliptical and monoclinic particles are considered. As the aspect ratio is an important parameter in determining whether rigid particles continually rotate or develop a stable orientation, both in theory (Ghosh and Ramberg, 1976) and in real mylonites (Pennacchioni et al., 2001; Mancktelow et al., 2002), this study specifically considers a range of aspect ratios ($R = 1–6$) of elliptical particles. For comparison, the kinematics of a monoclinic particle, more elongated than the one used in Mancktelow et al. (2002), is also investigated. Three experiments were also conducted to consider the influence of strain localization in the matrix adjacent to the particle (see ten Grotenhuis et al., 2002a). These experiments were very consistent and only one is presented here.

A complementary study (Schmid, 2002) applies finite element numerical modelling to the same general problem. Numerical modelling allows parameters to be varied continuously over a wide range to provide a proper sensitivity analysis. It also allows the flow field, stress and strain distribution to be investigated in detail. However, it is limited by practical problems of grid resolution to maximum shear strains of less than ca. 2–3. In contrast, analogue modelling is less flexible in varying parameters but particle behaviour can be studied to very large shear strains.

2. Experimental setup and theory

The experiments were carried out using a shear ring apparatus, described and used in Arbaret et al. (2001) and Mancktelow et al. (2002). The machine consists of two concentric cylinders of radii 18 and 30 cm that rotate in opposite directions around a central axis. This machine is capable of unlimited shear strain but does have a radial gradient in shear strain rate, for linear viscous materials given by:

$$\dot{\gamma} = \frac{-2(\dot{\Omega}_i - \dot{\Omega}_e)}{r^2\left(\frac{1}{r_i^2} - \frac{1}{r_e^2}\right)}, \quad (1)$$

where r_e and r_i are the external and internal cylinder radii and Ω_e and Ω_i the corresponding angular velocities (Reiner, 1969; Masuda et al., 1995). It follows that the amount of finite shear strain undergone by a particle depends on its radial position through time.

The matrix used is a transparent polydimethyl-siloxane polymer (PDMS SGM36 manufactured by Dow Corning). A 1.5-cm-thick layer of low-viscosity glycerine, acting as lubricant, underlies the PDMS layer. Experiments were conducted at a shear strain rate of $\sim 7 \times 10^{-4}\ s^{-1}$ (value measured at the centre of the particle) and at room temperature (ca. 22 °C). Under these conditions, the PDMS closely approximates Newtonian linear viscous behaviour, with a viscosity of ca. $3–5 \times 10^4$ Pa s (Weijermars, 1986; ten Grotenhuis et al., 2002b). Shear strain values γ of up to 45 (after 17 h) were attained during the

experiments. Digital photographs were taken at 5 min intervals.

The rigid particles were made of polypropylene with a density of 0.91. This is sufficiently close to that of the PDMS (0.97) to avoid significant vertical movements of the particle during an experiment. To simulate slip at the particle/matrix boundary, a weak lubricant layer (initially with approximately constant thickness) of liquid soap was added around the rigid particle (a technique first employed by Marques and Coelho, 2001). The enveloping layer extended below the particle, so that the particle was completely detached from the PDMS matrix. In most lubricated experiments, the volume of the soap layer is ca. 10% of the particle volume. In order to test the influence of the thickness of the weak layer on the rotational behaviour of the particle, some experiments were also prepared with soap volumes considerably more or less than 10% of the particle volume. For volumes of soap less than 5%, the exact value could no longer be accurately measured from the photographs. Liquid soap has a viscosity of 0.94 Pa s (determined by flow rate tests in a pipette), which is approximately 5×10^4 times less than that of the PDMS. The density is close to that of PDMS, so that no significant relative vertical movement of the soap layer occurred during the experiments. A regular grid was imprinted on the upper surface of the PDMS using a partially fixed photocopy (e.g. see Fig. 3 below; Dixon and Summers, 1985).

For the experiments, four cylindrical particles with different aspect ratios ($R = 1$, 2, 3 and 6) were employed, as well as a parallelepiped particle with a 2D monoclinic symmetry and aspect ratio of 5.4 for the NIH-image (http://rrsb.info.nih.gov/nih-image/) best-fit ellipse (Fig. 1). The monoclinic particle has a larger aspect ratio than the one ($R = 4.4$) used in Mancktelow et al. (2002). The cylindrical axis (c) of the particles was in all cases 2 cm in length. This axis was oriented parallel to the vorticity axis of the flow, i.e. perpendicular to the upper surface of the models. The long particle axis (a) also had a constant length of 3 cm for all the particles, whereas the length of the short axis (b) was varied to obtain different aspect ratios $R = a/b$ (Fig. 1a). The 3-cm-length of the particle long axis (elliptical) and diagonal (monoclinic) is small enough to avoid any significant effect of the shear strain gradient inherent in the ring-shear machine but large enough for accurate measurement of particle orientation from the digital photographs.

In the case of lubricated elliptical particles, different experiments were conducted for each particle aspect ratio, starting with the long axis at angles of approximately 0, 30, 60 and 90° to the shear plane. In practice, the actual initial orientation can differ from these ideal values (up to a maximum of 20° in one case), due to the difficulty of precisely positioning the particle in the presence of a soap layer. In the case of the lubricated monoclinic particle ($R = 5.4$), experiments were performed starting with the long diagonal of the particle nearly parallel to the shear plane.

The rotation history of the long axis (a) determined experimentally was then compared with that predicted by the Jeffery theory (1922), using the analytical solution of Fernandez et al. (1983):

$$\arctan(R\tan\alpha) - \frac{\gamma}{2}\sqrt{(1-\kappa^2)} = \arctan(R\tan\alpha'), \tag{2}$$

where $R = a/b$ is the aspect ratio of the particle, α and α' are the orientation of the long axis (a) of the particle before and after shear strain γ (see Fig. 1) and κ is a shape factor given by Willis (1977):

$$\kappa^2 = \frac{R^2 - 1}{R^2 + 1}, \tag{3}$$

3. Results

3.1. Elliptical particles without interface lubrication

PDMS is very sticky so that bonding across the interface in unlubricated experiments was good and interface slip was avoided. In Fig. 2, the results of these series of experiments are compared with the 2D analytical solution of the Jeffery equation (Eq. (2)). The measured curves for the particles with aspect ratio 1 and 2 perfectly fit the theoretical ones, while more elongated particles (aspect ratio 3 and 6) rotate slightly faster than the theory predicts. The deviation of experimental results from the theoretical solution increases with increasing aspect ratio. This slight difference in the rotational behaviour, which was also observed in the experiments of Mancktelow et al. (2002), may be due to the shear gradient present in the ring shear machine.

3.2. Elliptical particles with interface lubrication

The introduction of slip at the particle/matrix boundary led to considerable deviation of the measured rotation paths from the theoretical ones. These deviations depend on both the initial orientation of the particle and on the thickness of the weak layer surrounding the particle. The thickness of the weak layer, which was initially approximately constant, obviously changes during the experiments and becomes unevenly distributed, progressively forming elongate thin tails extending into the matrix (Fig. 3).

For circular particles ($R = 1$), the rotation rate ($\delta\alpha/\delta\gamma$) is nearly identical to the theoretical one up to $\gamma = 2$ (Fig. 4a and b). With further shear, the rotation rate rapidly increases to stabilise at a value higher than the theoretical one (Fig. 4b).

For aspect ratio $R = 2$, the particle kinematics are strongly influenced by the initial orientation (Fig. 5). When the long axis of the particle is initially oriented parallel to the shear plane (Experiment 10: Fig. 5a), the particle rotates

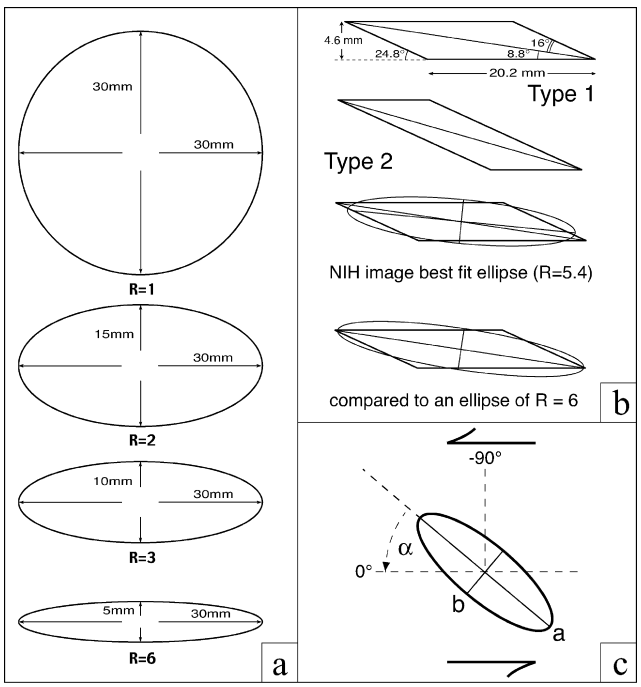

Fig. 1. Cross-sectional shape of the rigid particles used for the experiments. In each case, the third axis, which is placed parallel to the vorticity axis in the shear flow, is 2 cm in length. (a) Circular and elliptical particles with aspect ratios 1, 2, 3 and 6. (b) Monoclinic particle: the two upper figures illustrate the type 1 and type 2 particle symmetry during sinistral shear; the best fit ellipse calculated with NIH image and, for comparison, an ellipse of aspect ratio 6 are shown in the lower two figures. (c) Convention used for the angle α in Eq. (2) and in the plots.

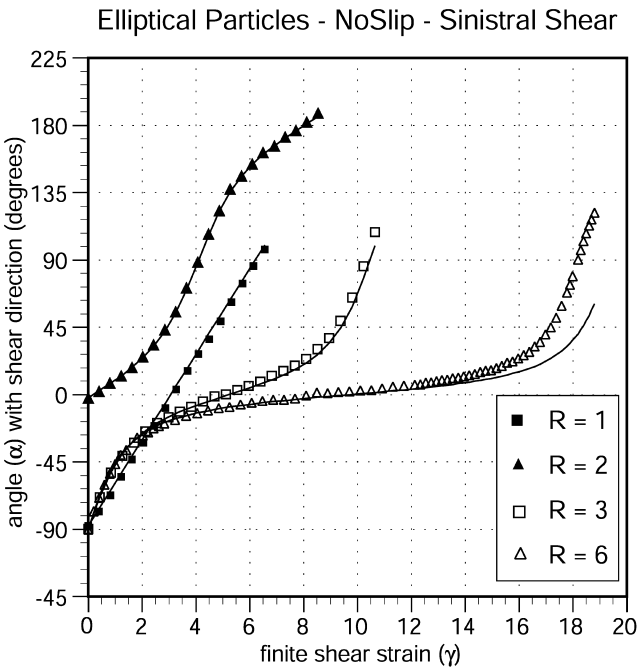

Fig. 2. Rotational paths of the long axes of elliptical particles with aspect ratio 1, 2, 3 and 6, in unlubricated experiments. Solid lines represent the theoretical rotation curves calculated with Eq. (2). The shear strain indicated in the graphs was determined at the centre of the particle.

backwards (antithetically) during the first strain increments. At $\gamma = 0.6$, the particle reaches a metastable position, maintained until $\gamma = 2$, with its long axis at an angle of $-16°$ to the shear plane. With increasing shear, the particle starts to rotate synthetically and passes through the initial orientation at $\gamma = 4.7$, still continuing to rotate synthetically. After a 180° rotation, when the particle long axis is again oriented parallel to the shear plane ($\gamma = 11.5$), the particle continues its forward rotation with no tendency for back rotation (Fig. 5a). In contrast, the particles with other initial orientations only rotate forwards (Fig. 5b and c) and their rotational behaviour only differs slightly from the theoretical one. In the case of an initial inclination α_0 of $-25°$ (Experiment 13: Fig. 5b) and $-40°$ (Experiment 19: Fig. 5c), the particle behaviour is very close to the theoretical one, whereas for an initial orientation of $-90°$ (Experiment 12: Fig. 5b) the particle rotates slightly faster. Fig. 5c shows both the forward and reverse rotation paths produced by reversing the shear sense from sinistral to dextral midway through Experiment 19. The reverse path is very similar to the forward one, establishing that the experiment is effectively reversible.

For aspect ratio $R = 3$, the particle kinematics (Figs. 6 and 7) show strong similarities to those described for particles of aspect ratio 2. Also in this case, when the particle long axis is initially parallel to the shear zone, the particle first rotates backwards (Experiments 14 and 29: Figs. 6a and 7a and b). To test the influence of the soap thickness, the experiment with an initial angle $\alpha_0 = 0°$ was repeated: (i) with a large amount of soap (ca. 13% of the particle volume: Experiment 14 in Fig. 6a), and (ii) with a very thin soap layer (thickness not optically measurable: Experiment 29 in Fig. 6a). In both experiments, the maximum angle of back rotation is smaller than in the case of the particle with $R = 2$. In the case of a thick soap layer, the particle reaches a metastable position from $\gamma = 1$ to $\gamma = 2$, with the long axis at an angle of $-10°$ to the shear plane. For $\gamma > 2$, the particle starts to rotate synthetically and the long axis passes through the shear plane at $\gamma = 4.2$. In the case of a very thin soap layer, the particle first rotates backwards until the long axis reaches an angle of $-16°$ to the shear plane at $\gamma = 1.2$. It then starts to rotate forwards, with the long axis passing through the shear plane at $\gamma = 5.5$. In other words, the particle with a thin soap layer rotates considerably slower than the one with a thick soap layer. This difference in the rotation rate becomes more evident after a 180° particle rotation. The long axis approaches the shear plane again for $\gamma = 15$ in the first case (Experiment 14) but only after $\gamma = 18.2$ in the second case (Experiment 29). Therefore, a 180° rotation requires a shear strain γ of 12.7 (from $\gamma = 5.5$ to $\gamma = 18.2$) for a thin soap layer and 10.8 (from 4.2 to 15) for a thick soap layer. In these experiments, there was no evidence of back rotation each subsequent time the particle long axis passed through the shear plane.

A third curve plotted in Fig. 6a (Experiment 25) shows

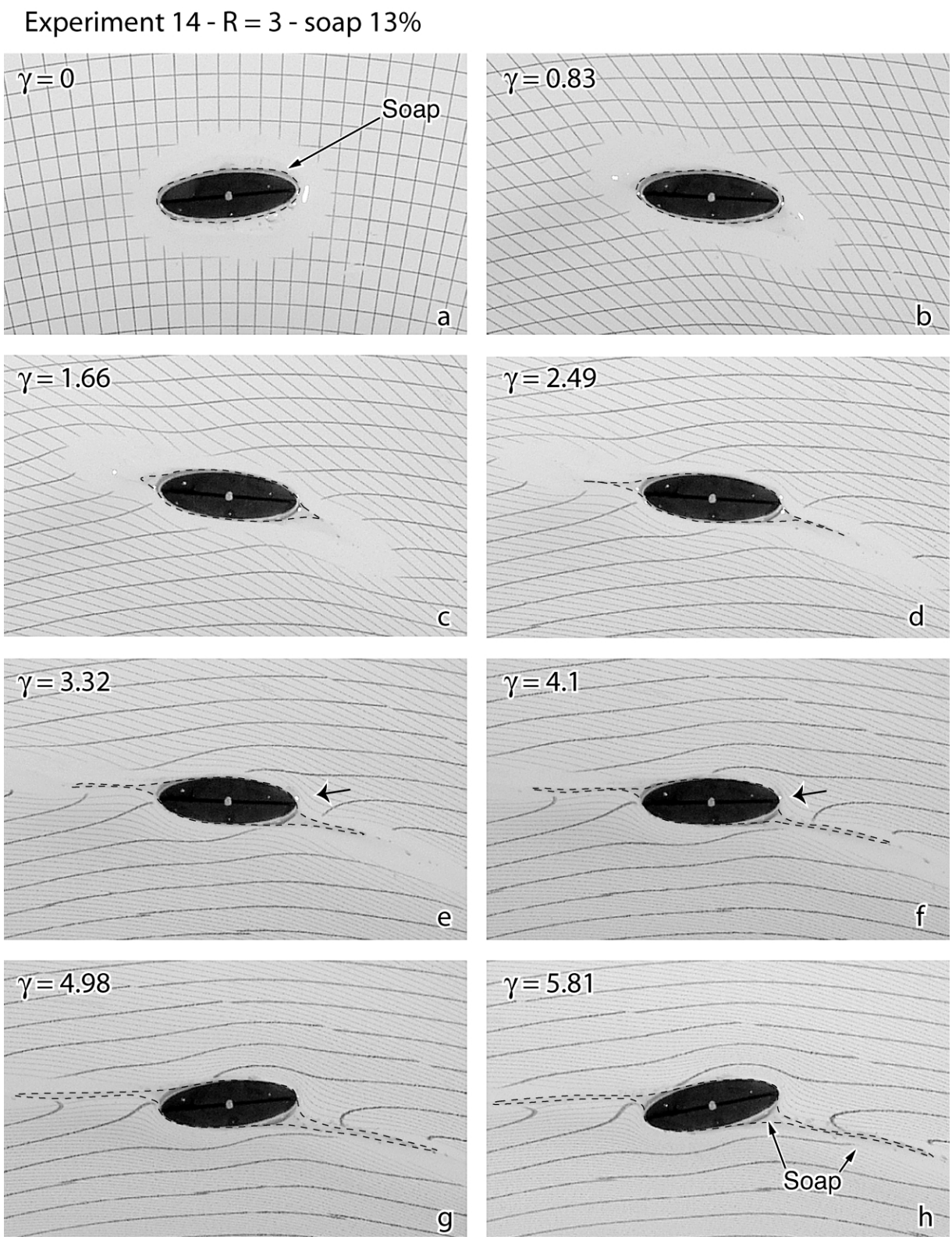

Fig. 3. (a)–(h) Series of photographs at 20-min-intervals for Experiment 14 showing the rotational behaviour of the particle and the evolution and thinning of the weak layer surrounding the particle. The shear plane is horizontal and the shear sense sinistral.

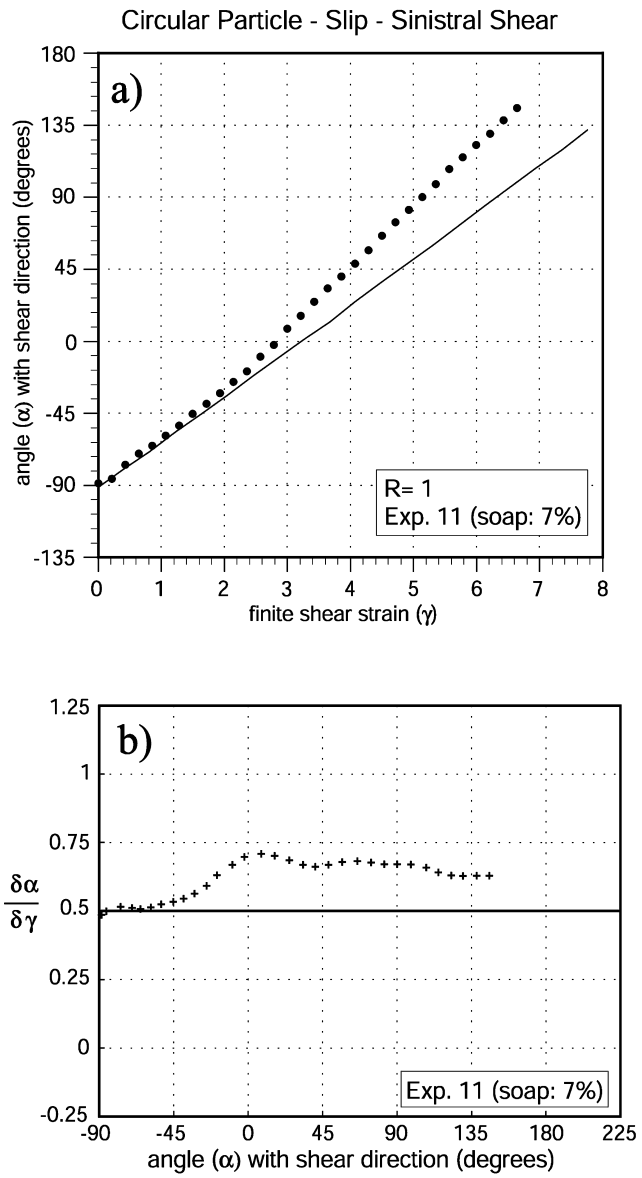

Fig. 4. (a) Rotational path of a lubricated circular particle (Experiment 11, $R = 1$), with the solid line representing the appropriate theoretical path. (b) Rotation rates ($\delta\alpha/\delta\gamma$) calculated for the same experiment compared to the theoretical values.

the rotational behaviour of a particle with the same aspect ratio (3) and starting orientation ($\alpha_0 = 0^\circ$) as in the previous experiments. However, in this case slip did not occur at the particle/matrix interface but instead strain localization was induced in the matrix close to the particle. The initial setup involved placing the particle directly in the PDMS (as for the unlubricated experiments) and then producing two cuts on either side of the particle, which were filled with soap. The two cuts were at a distance of ~1 cm from the particle centre, had a length of ~15 cm and a depth of ~3 cm (i.e. the cut extends in the matrix 1 cm deeper than the particle) and were subparallel to the shear plane. This experimental setup did not produce any significant deviation of the particle behaviour from the theoretical one. In contrast with

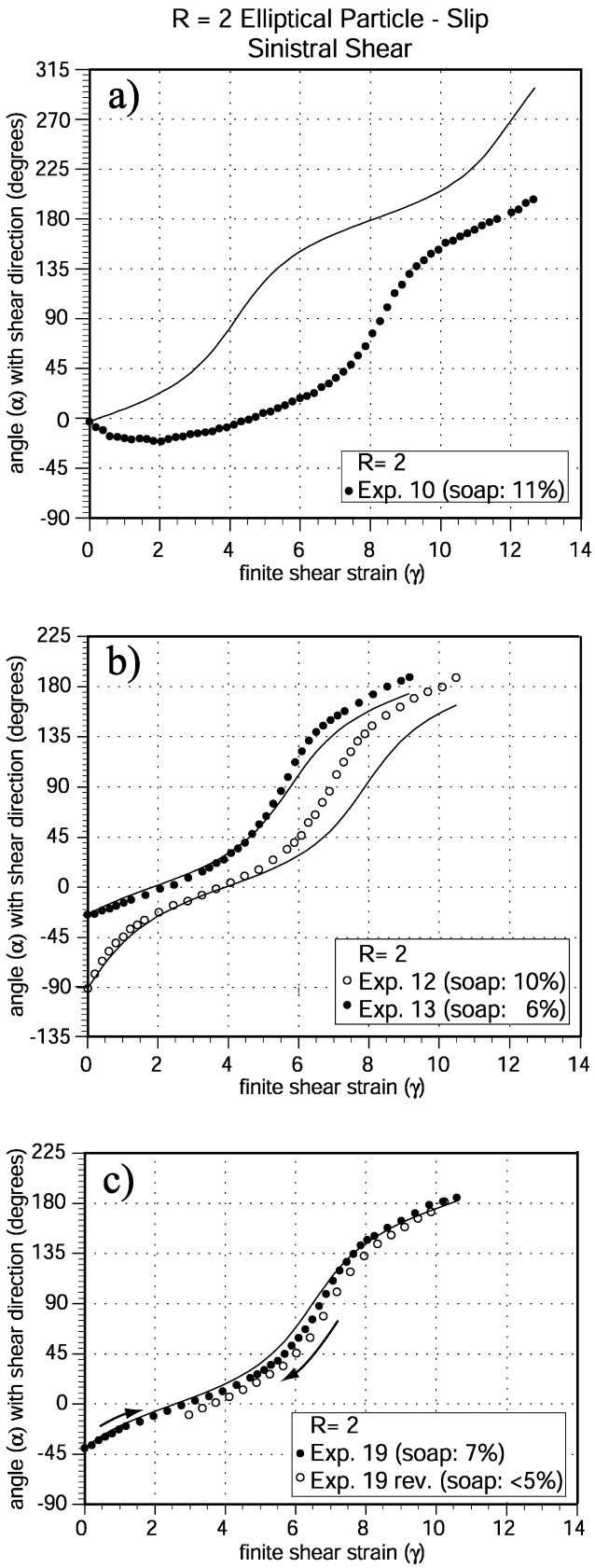

Fig. 5. Rotational paths of an elliptical particle with aspect ratio $R = 2$ and a lubricated boundary. Solid lines represent the calculated theoretical path. (a) Experiment 10. (b) Experiments 12 and 13. (c) Experiment 19, forward (black dots) and reverse (open circles) runs.

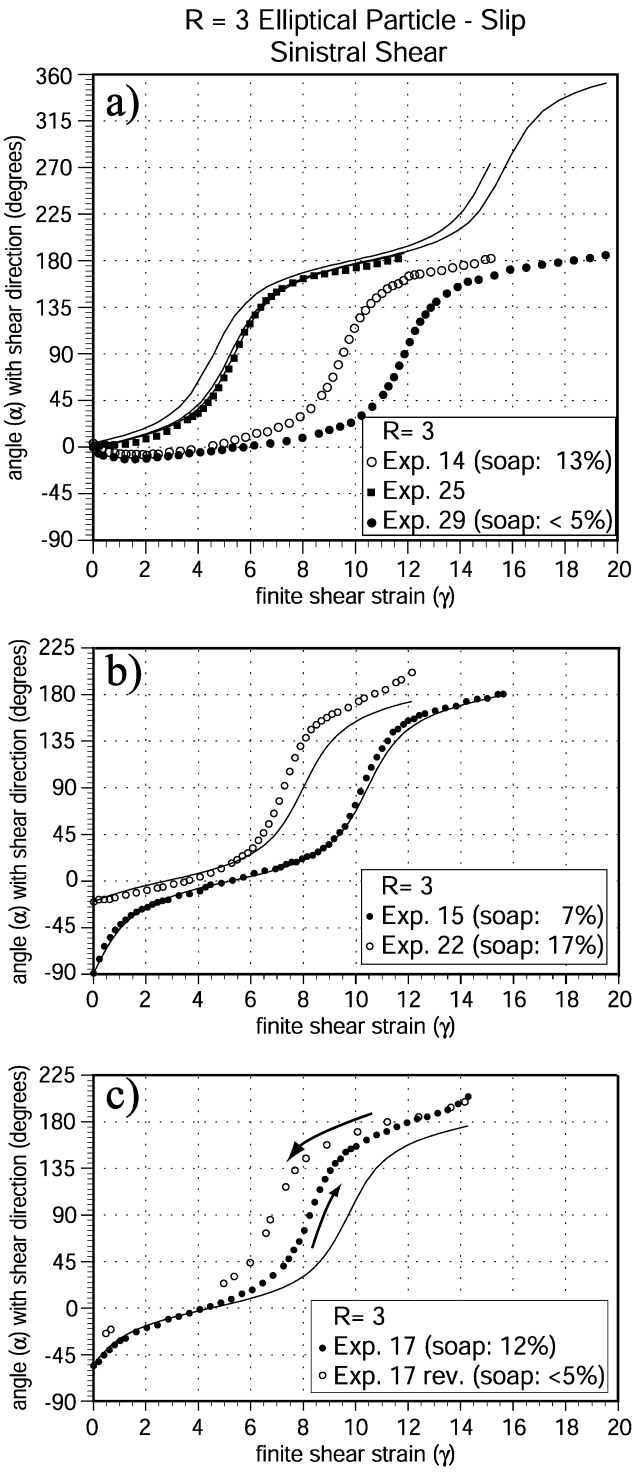

Fig. 6. Rotational paths of an elliptical particle with aspect ratio $R = 3$ and lubricated boundary. Solid lines represent the calculated theoretical path. (a) Experiments 14, 25 and 29. (b) Experiments 15 and 22. (c) Experiment 17, forward (black dots) and reverse (open circles) runs.

what was observed in the case of lubricated particles, localization in the adjacent matrix does not induce backward rotation.

For all other initial positions different from $\alpha_0 = 0°$ (see Fig. 6b and c), the particle always rotates only in a forward sense. In these experiments the rotation rate is either nearly identical to the theoretical one (Experiment 15: Fig. 6b), or the particles appear to rotate faster than the theory predicts (Experiments 17 and 22: Fig. 6c and b). However, a correct analysis of the results must also take into account the differences in the initial thickness of the soap mantle in the various experiments.

The influence of the thickness of the weak layer on the particle kinematics is particularly evident in some experiments. In Experiment 22 (Figs. 6b and 7c) and Experiment 17 (Figs. 6c and 7d), where the volume of soap is higher than 10% of the particle volume, the 'instantaneous' rotation rate of the particle is significantly faster than the theory predicts during the entire experiment, once synthetic rotation has been established. This effect is not so evident in Experiment 14 (soap 13% of particle volume). In this experiment, after the initial stage of back rotation ($\gamma = 0$–4.2; Figs. 3a–f and 6a), the particle shows increased instantaneous rotation rates with respect to theory only when the particle long axis is at a high angle to the shear plane (Fig. 7a). As a result, there is only a very small difference in the required γ for a complete 180° rotation compared with theory (10.8 vs. 10.2). In contrast, when the soap layer around the particle is very thin (Experiment 29 in Figs. 6a and 7b; Experiment 15 in Figs. 6b and 7e), the rotation rate is higher than the theoretical one when the particle long axis is oriented at a high angle to the shear plane, but lower when the particle long axis is at a low angle to the shear plane (Fig. 7b). It is also noticeable that the particle rotation rates during the reverse experiment (Experiment 17 in Figs. 6c and 7f) are reduced compared with the forward run.

In the case of particles with aspect ratio $R = 6$, experiments had to be run to very high shear strains ($\gamma = 45$, corresponding to an experiment duration of 17 h) because of the very slow rotation rates when the long axis of the particle was close to the shear direction (Figs. 8 and 9). In these experiments, results are similar to those described for less elongated particles, but the deviation from the theoretical curves is more marked.

Starting with the particle long axis parallel to the shear zone (Experiment 16 in Figs. 8a and 9a), an initial backward rotation is observed. The particle reaches an angle of −20° after a finite strain of $\gamma = 3$ (Fig. 8a) and then immediately starts to rotate forward. At $\gamma = 7.5$, the particle long axis is again parallel to the shear zone and continues to rotate forward until it reaches the shear plane for a second time at $\gamma = 32$. The particle therefore required $\gamma = 24.5$ (from 7.5 to 32) for a 180° rotation, which is more than in the case of unlubricated particles ($\gamma = 18.2$), which are close to the theoretical case ($\gamma = 19.3$). The second time the particle long axis approaches the shear plane (from γ ca. 27–32) after a 180° rotation, it rotates considerably slower than the first time (from γ ca. 5–7.5), as is evident from comparison of the curve slopes in Figs. 8a and 9a.

In all the other experiments with an initial particle

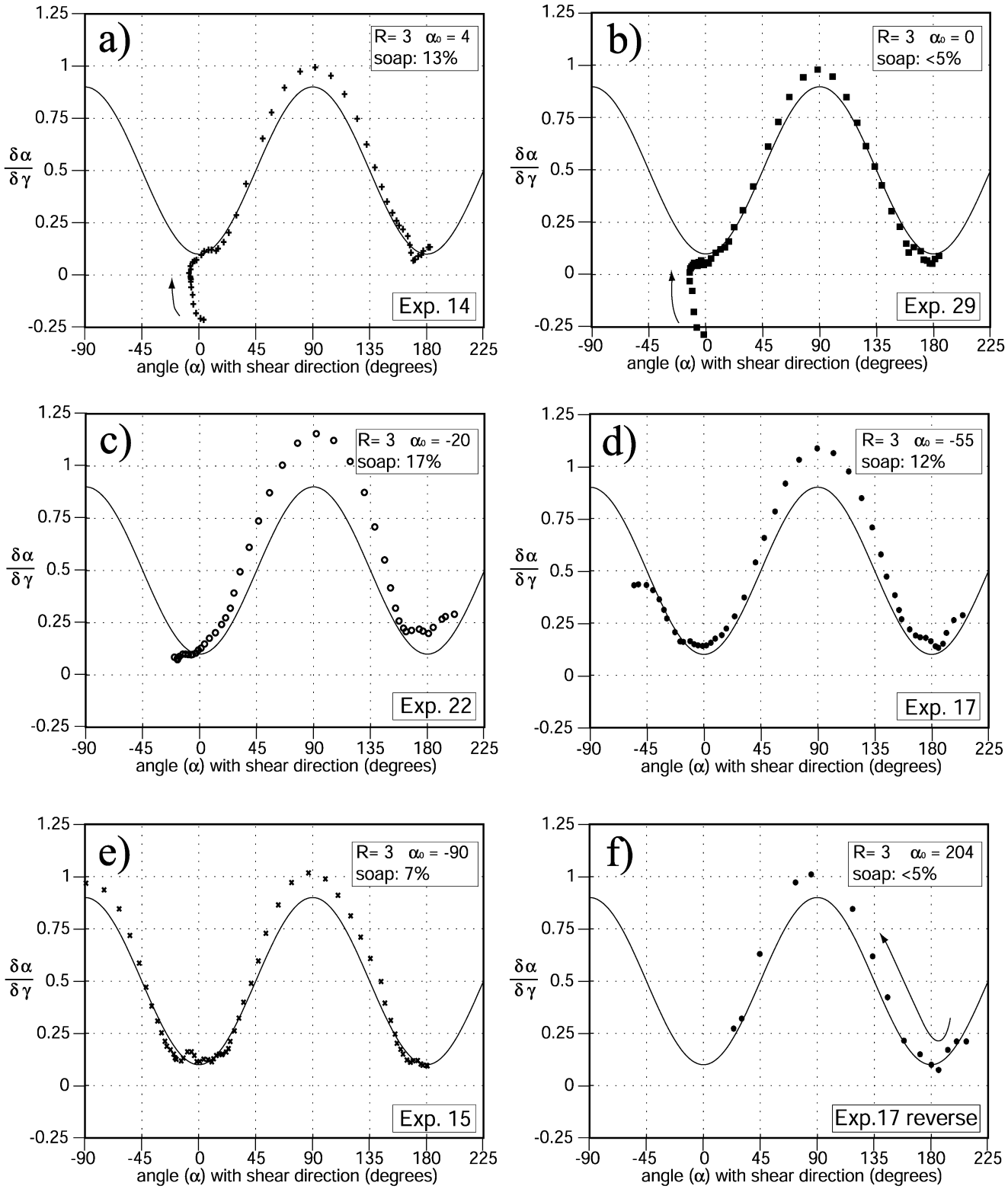

Fig. 7. Rotation rates for experiments with an elliptical particle of aspect ratio $R = 3$. (a) Experiment 14. (b) Experiment 29. (c) Experiment 22. (d) Experiment 17. (e) Experiment 15. (f) Experiment 17 reverse. The amount of soap used is indicated in volume percent relative to the particle size for each of the experiments. α_0: initial orientation.

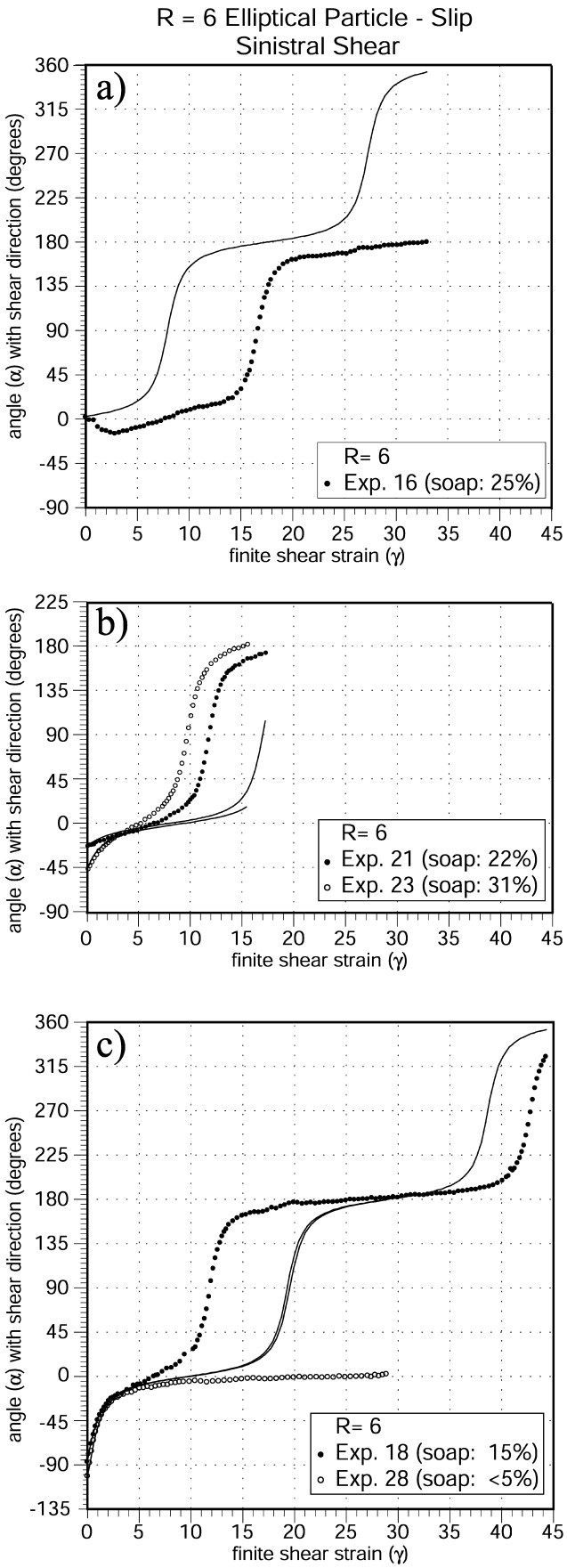

Fig. 8. Rotational paths of an elliptical particle with aspect ratio $R = 6$ and lubricated boundary. Solid lines represent the calculated theoretical path. (a) Experiment 16. (b) Experiments 21 and 23. (c) Experiments 18 and 28.

orientation different from 0° (Experiments 18, 21, 23, and 28), the particle only rotates forwards (Fig. 8b and c). Fig. 10a–f presents a direct comparison of Experiments 21 ($\alpha_0 = -30°$) and 23 ($\alpha_0 = -45°$) for $\gamma = 0$, $\gamma = \sim 2.5$ and $\gamma = \sim 5$. In both experiments, a thick soap layer was used and the rotation rate during the whole experiment is always equal to or greater than the theoretical one, irrespective of the orientation of the particle (see Fig. 9b and c). As can be seen in Figs. 8b and 10, the particle rotates faster in Experiment 23 (with a larger amount of soap), than in Experiment 21.

Two further experiments (Experiments 18 and 28) were performed with the same initial particle orientation $\alpha_0 = -90°$ but different thickness of the weak layer, namely 15% (Experiment 18: Figs. 8c and 9d and f) and very thin (less than 5% in Experiment 28: Figs. 8c and 9e). In Experiment 18, the particle makes two 180° rotations, requiring a shear strain of $\gamma = 11.9$ (from 0.1 to 12) for the first rotation and a shear strain of $\gamma = 31$ (from 12 to 43) for the second one. When the particle long axis crosses the shear plane the first time (after a 90° rotation), its rotation rate is higher than the theoretical one, whereas the second time the particle approaches the shear plane (and the soap layer has already become very thin) the particle rotates significantly slower than theory predicts (Fig. 9d). As was seen for most of the lubricated experiments, the rotation rate of the particle is greater than the theoretical value when it is oriented with the long axis at a high angle to the shear plane. However, when the weak layer is already very thin from the beginning, the particle rotates considerably slower than theory predicts during the first rotation through the shear plane (Fig. 9e).

3.3. Monoclinic particles with interface lubrication

One experiment (Experiment 26) with a monoclinic particle of aspect ratio 5.4 (NIH-image best-fit ellipse, see Fig. 1) was performed starting with the long diagonal of the particle nearly parallel to the shear plane. Because of the lack of point symmetry in monoclinic particles, there are two possible geometries depending on whether the short or long side of the rhomboidal particle is the first to come into near parallelism with the plane of shearing. In type 1, it is the long side, in type 2 it is the short side (see Mancktelow et al., 2002). In Experiment 26, the geometry was of type 2. As already described in Experiment 3 of Mancktelow et al. (2002) (where a lower aspect ratio particle with $R = 4.4$ was used), and confirmed in Experiment 26 of this study, the particle rotates backward and slowly approaches a stable position. In Experiment 26 it stabilizes after a shear strain of $\gamma = 5.2$ (Fig. 11) with its long diagonal making an antithetic

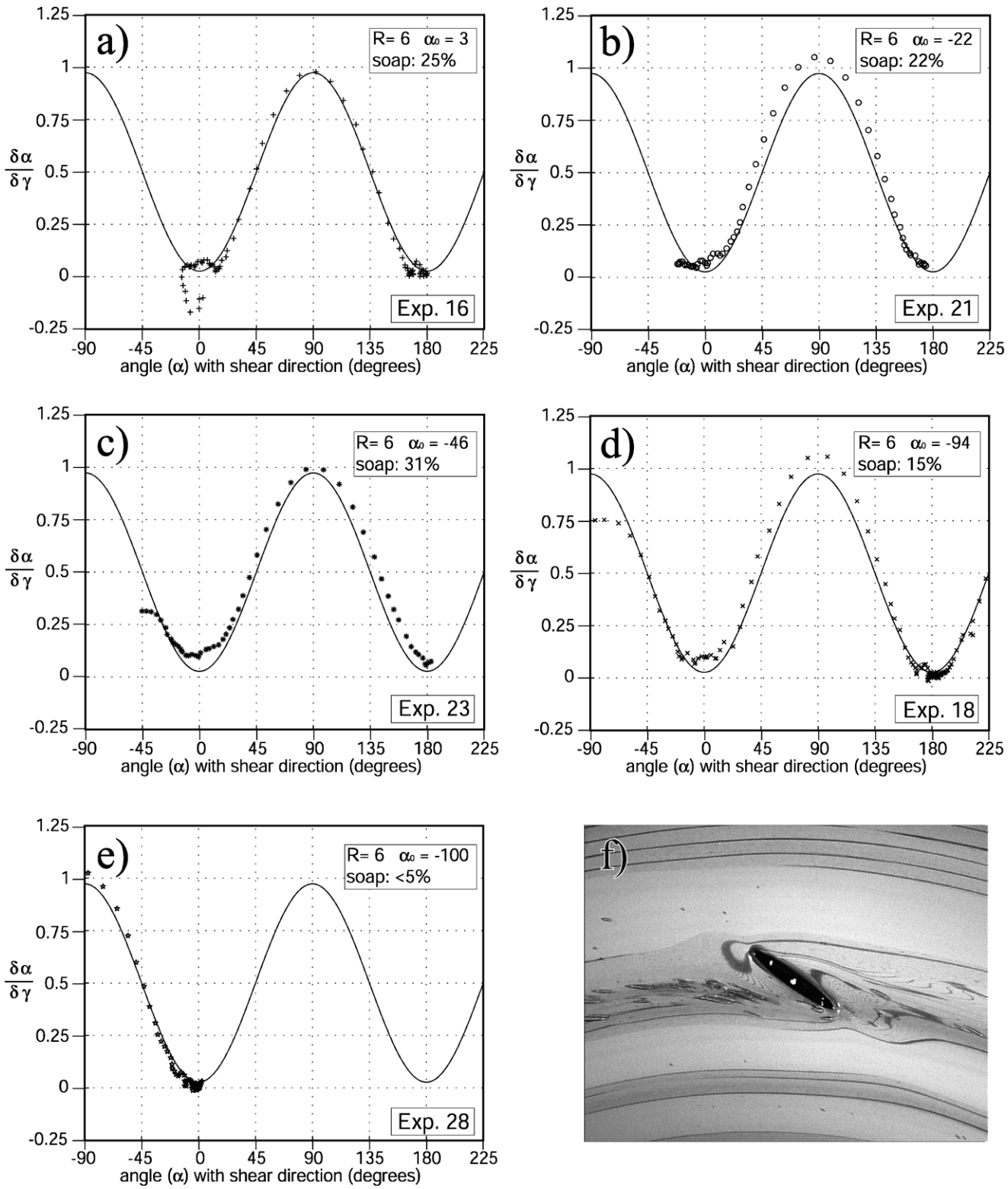

Fig. 9. Rotation rates for the experiments with an elliptical particle of aspect ratio $R = 6$. (a) Experiment 16. (b) Experiment 21. (c) Experiment 23. (d) Experiment 18. (e) Experiment 28. The amount of soap used is indicated in volume percent for each of the experiments. α_0: initial orientation. (f) Photograph of the final position of the particle in Experiment 18 (shear plane is horizontal, shear sense sinistral).

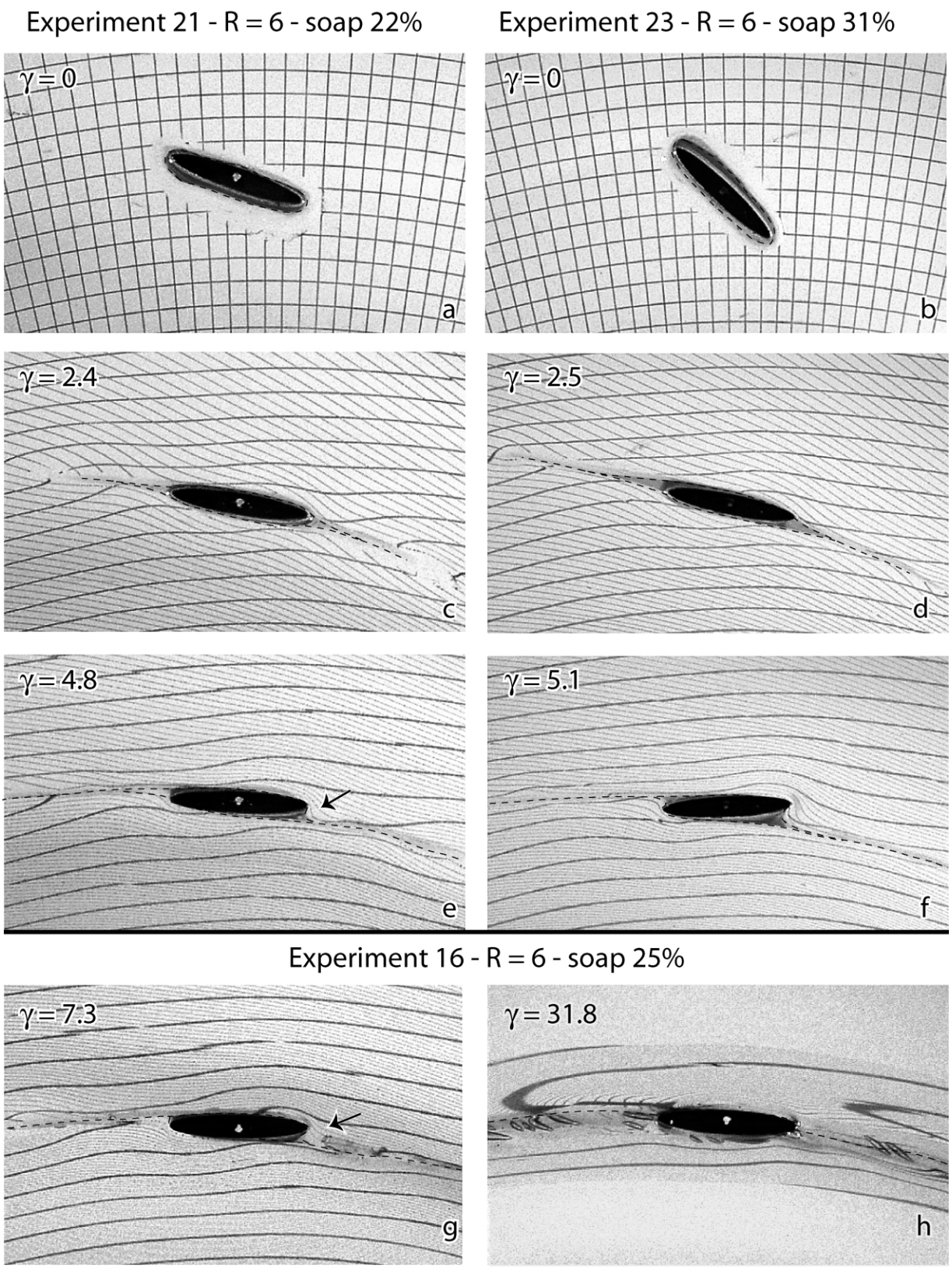

Fig. 10. (a)–(f) Series of photographs at 1-h-intervals, comparing the rotational behaviour of the particle and the thinning of the surrounding weak layer for Experiment 21 ((a), (c) and (e)) and Experiment 23 ((b), (d) and (f)). (g) Photograph, 3 h after starting, for Experiment 16 showing the weak layer surrounding the particle when it approaches the shear plane for the first time ($\gamma = 7.3$). (h) Photograph showing the thinning of the weak layer after 13 h for the same experiment ($\gamma = 31.8$), when the particle approaches the shear plane for a second time. In all photographs, the shear plane is horizontal and the shear sense sinistral.

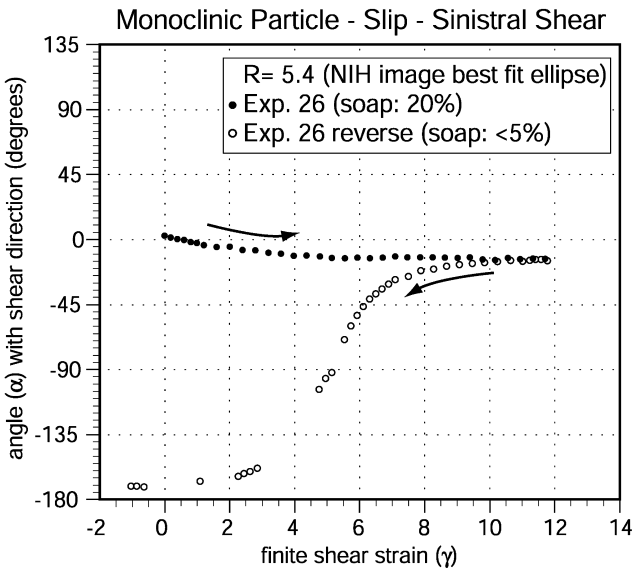

Fig. 11. Rotational paths of a monoclinic particle with aspect ratio 5.4 (best-fit NIH image) and lubricated boundary. Black dots represent the forward experiment (Experiment 26) and open circles represent the reverse experiment (Experiment 26 reverse).

angle of $-12°$ with the shear plane and its short straight side nearly parallel to the shear plane. With increasing strain (up to $\gamma = 12$; Fig. 12a) the particle remains stable in this orientation and does not start to rotate forward. The experiment was also reversed, with a concomitant change in the particle symmetry from type 2 to type 1. When inverting the shear sense (i.e. now dextral shear), the monoclinic particle remains nearly stable (a continuous but very slow rotation is visible) for an increment of $\gamma = 1.8$ and then starts to rotate synthetically with the sense of shear. The particle rotates 157° until it approaches the shear plane again after a finite strain $\gamma = \sim 11$ and acquires a new stable position, now with its long diagonal making an antithetic angle of 10° to the shear plane and its long side effectively parallel to the shear plane.[1] It is therefore clear that monoclinic rhomboidal particles behave quite differently from elliptical particles. In particular, the experiment is not reversible and in both normal and reverse experiments the particle long axis never crosses the shear plane.

4. Discussion of the analogue experiments

The experiments presented above show that the rotational behaviour of an elliptical particle with a lubricated particle/matrix interface is influenced by three main parameters: (1) its initial orientation with respect to the shear plane; (2) the volume of the weak soap mantle around the particle; and (3) the aspect ratio.

[1] Note that the mathematical convention that anticlockwise angles are positive is always followed, with the result that antithetic angles are negative in sinistral shear and positive in dextral shear.

The experiments produced very consistent results concerning the influence of the initial orientation of the particle. In contrast with unlubricated particles, which closely follow the theoretical paths, all lubricated particles initially oriented with their long axis parallel to the shear direction rotate backwards (antithetically) during the first increments of strain (see Experiment 10 in Fig. 5a, Experiments 14 and 29 in Fig. 6a and Experiment 16 in Fig. 8a). With increasing strain, the particles first temporarily stabilize at an angle between 10 and 20° to the shear plane and then start to rotate synthetically. The antithetic rotation only takes place during the first stages of the experiments. A subsequent period of back rotation is not observed when, after a further 180° rotation, the particle long axis again passes across the shear plane. Similarly, a back rotation effect is not observed during reversal of Experiments 17 and 19, where the particles were oriented with their long axis close to the shear plane when the shear sense was inverted. A clear explanation for this change in behaviour of the particles cannot be deduced directly from the analogue experiments. However, the numerical results of Schmid (2002) establish that back rotation should only occur when the thickness of the weak layer exceeds a minimum critical value. According to Schmid (2002), this critical value is a function of the viscosity contrast between matrix and lubricant mantle, with the critical thickness increasing with decreasing viscosity contrast. For a lubricant viscosity 5×10^4 times less than the matrix, as was the case for the current analogue experiments, this critical value should be 2% of the volume of the particle. Because of the physical limitations in preparation of the analogue experiments, the starting thickness of the weak layer always exceeded this minimum critical value, inducing initial back rotation of the particle. However, in the course of the experiments, strain-induced thinning of the weak layer reduces the thickness of the weak mantle directly surrounding the particle to values below the critical one. As a result, second and subsequent 180° rotations of the particle no longer show back rotation when the long axis is close to the shear direction (Fig. 3).

These changes in soap distribution and thickness can be seen in Fig. 3, where the first stages of backward rotation are accompanied by a rapid thinning of the soap layer as it initially extends into the direction of maximum elongation (Fig. 3b and c). With increasing strain, tails are developed (Fig. 3d and e) and the soap is continuously removed from the mantle surrounding the particle into the extending tails, which become increasingly parallel to the shear plane (Fig. 3f–h, see also Taylor, 1934).

Synthetic rotation is observed from the very first strain increments for all initial particle orientations different from $\alpha_0 = 0°$ that were considered in this study (i.e. $-30°$, $-60°$ and $-90°$), irrespective of the aspect ratio. However, the presence of a weak mantle around the particle may provoke significant deviation of the particle behaviour from that of unlubricated particles and, therefore, from the Jeffery (1922) theory. The previous study of Mancktelow et al.

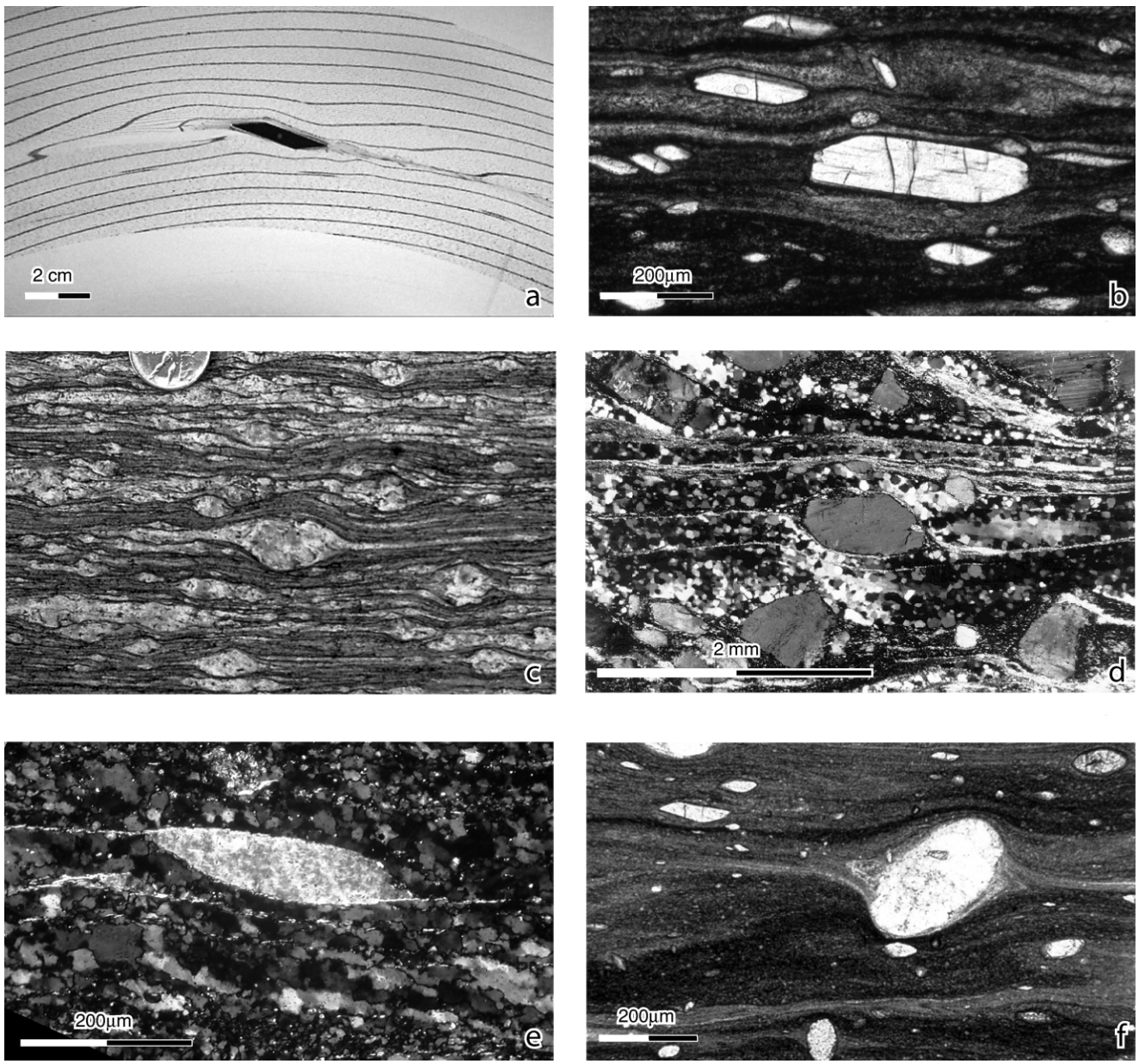

Fig. 12. (a) Photograph at $\gamma = 9.2$ for Experiment 26 showing the final stable position of the particle, with its long axis at a low antithetic angle to the horizontal shear plane (shear sense sinistral). (b) Photomicrograph of type 2 rhomboidal porphyroclasts of prismatic sillimanite showing a strong SPO in the Mont Mary mylonites (Alps, Italy). Note the similar orientation of the prismatic sillimanite to the rigid particle in (a). (c) Photograph of type 1 feldspar porphyroclasts from the border of the Monte Rosa nappe, Villadossola (Alps, Italy). (d) Photomicrograph of type 1 feldspar porphyroclasts (fig. 5.20 from Passchier and Trouw, 1996). (e) Photomicrograph of mica fish from a quartz-rich mylonite of the Dent Blanche nappe (Western Alps). (f) Photomicrograph of elliptical plagioclase and garnets and rhomboidal sillimanite in the Mont Mary mylonites (Alps, Italy); note the random orientation of the small garnet porphyroclasts and the complex tail geometry of the large plagioclase porphyroclast in the centre of the photograph.

(2002) indicated that an elliptical particle of aspect ratio 5.3 with lubricated boundaries rotates slower than the same particle without slipping boundaries. This is not always true in the present experiments. In some cases the particles do indeed rotate slower than theory predicts (Experiments 16, 18, 28 and 29), while in other cases they rotate at rates close to the theoretical values (Experiments 13, 15 and 19) or even faster (Experiments 12, 17, 21, 22 and 23). An analysis of the different experiments indicates that the difference in the rotational behaviour depends on several factors: (i) the initial volume of weak material present around the particle; (ii) the aspect ratio of the particle; and (iii) the amount of bulk shear strain. In all experiments with a weak particle mantle initially exceeding 10% of the particle volume, the bulk rotation rate of the particles is faster than the theory predicts, irrespective of the particle aspect ratio (Experiment 12: Fig. 5b; Experiment 22: Fig. 6b; Experiment 17: Fig. 6c; Experiments 21 and 23: Fig. 8b; Experiment 18: Fig. 8c). For thin weak mantles (i.e. less than 10% of the particle volume; Experiment 13: Fig. 5b; Experiment 19:

Fig. 5c; Experiments 15 and 22: Fig. 6b; Experiment 28: Fig. 8c), the particles rotate slower than in experiments with a thicker soap layer and the less elongate particles (i.e. aspect ratio 2, see Experiments 13 and 19: Fig. 5b and c) show a rotational behaviour similar to theory. For the same thin weak layer, more elongated particles (aspect ratios 3 and 6) rotate even more slowly and indeed slower than the Jeffery theory predicts. For example, the particle with aspect ratio 3 produces rotational curves similar to the theoretical one in the presence of a weak layer representing 7% of the volume of the particle (Experiment 15 in Fig. 6b), but the same particle rotates slower than theory when the weak layer becomes very thin (see Experiment 29 in Fig. 6a). The strongly elongate particle ($R = 6$) rotates considerably slower than the theory predicts in the presence of a small amount of weak material (Experiment 28 in Fig. 8c).

During the experiments, the thickness of the weak mantle around the particle is progressively reduced and therefore the lubrication conditions change with increasing γ (Figs. 3 and 10). This could explain the progressive decay in rotation rates observed during some experiments, which would be consistent with thinning the soap mantle. For example, in Experiments 16 (Figs. 8a and 9a) and 18 (Figs. 8c and 9d and f), which accumulate the highest γ, the particles rotate at higher instantaneous rotation rates (compared with theoretical ones) the first time the long axis passes through the shear plane (after $\gamma = 7.5$ and 11.9, respectively; Fig. 10g) than the second time ($\gamma = 32$ and 31; Fig. 10h) when the soap mantle has thinned to values much less than 1%. Figs. 3 and 10 also provide a possible qualitative explanation for the influence of the thickness of the soap layer on the rotational behaviour of the particle. When the particle long axis approaches the shear plane for the first time (see Fig. 10e and g), the soap still present at the particle–matrix interface migrates into 'pressure shadow' locations that are displaced relative to the particle tips. This allows the matrix to flow around the tips of the particle (see arrows in Figs. 3e and f and 10e and g) before its long axis has actually passed through the shear plane, which probably increases the traction on the particle and hence its rotation rate, as observed in Experiments 16, 18, 21 and 23. When, in Experiments 16 and 18, the particle approaches the shear plane for the second time, the soap layer has already been considerably thinned and this behaviour is not observed (Fig. 10h). For very thin films of soap, channel-like flow from the mantle into pressure shadows is hindered by the narrow width of the channel and the small volume of weak material still available. In this case, the matrix continues to flow undisturbed around the particle until its long axis has passed through the shear plane and the instantaneous rotation rates are actually lower than the theoretical ones, because of reduced traction across the slipping interface.

The continuous thinning of the soap layer observed during all the experiments could also be invoked to explain the 'anomalous' behaviour observed in Experiment 14 (Figs. 3 and 7a). Here the rotation rates during the 0–180° rotation are lower compared with Experiments 22 (Fig. 7c) and 17 (Fig. 7d), even though the initial soap mantle thickness is similar. Because of the initial stage of back rotation in Experiment 14, the particle has already experienced a significant shear strain and corresponding mantle thinning before it regains the initial position at $\alpha = 0°$ (Fig. 3f), so that its behaviour during the subsequent full rotation (0–180°) is more comparable with that of a particle with a thin soap mantle. Further evidence for a slow down in particle rotation rates with decreasing mantle thickness is provided by Experiment 17, where rotation rates during the reverse experiment, and therefore after a certain thinning of the soap mantle, are lower than during the forward run (Figs. 6c and 7d and f). This effect is not evident for the lower aspect ratio particle ($R = 2$: Experiment 19 forward and reverse), for which the rotation curves in both the forward and reverse experiments are almost identical and very similar to the theoretical one. In Experiments 17 and 19, the shear sense was inverted when the particle was parallel to the shear plane for a second time, i.e. after a 225° rotation. This 225° rotation is reached at a lower γ in the case of $R = 2$ than for $R = 3$ and therefore there was less thinning of the soap mantle for the lower aspect ratio particle, which could explain the observed differences between the two experiments.

From the present study it can be deduced that all elliptical particles tend to rotate faster in the presence of a thick weak layer surrounding them. However, when the weak layer is very thin, the more rounded particles rotate slower than in the presence of a thicker weak layer, but not slower than the theory predicts, whereas particles with a high aspect ratio and a very thin weak layer rotate considerably slower than the theory predicts (though never zero!). In detail, the rotation rates are slower than the theoretical ones only when the long axis lies at a low angle to the shear plane (see Figs. 7b and e, 9a, d and e). As a consequence, elongated particles spend a very long time with their long axis at a low angle to the shear direction, developing a quasi-stable orientation. More rounded particles instead never show rates slower than the theoretical ones.

Using the same experimental set up, a monoclinic particle with lubricated boundaries (Experiment 26 in Fig. 11) asymptotically approaches a stable position with its long axis at a low angle to the shear plane. Depending on the symmetry of the particle, the antithetic angle varies from ca. 10° in the case of a Type 1 monoclinic particle (see Fig. 1b, dextral shear) to ca. −12° in the case of a Type 2 particle (Fig. 1b, sinistral shear, see also footnote 1). In summary, an elliptical particle embedded in a Newtonian matrix undergoing simple shear never reaches a true stable position, while a monoclinic one does. This indicates that stabilization of an elongated object is due to the combined effect of slip on the boundary and shape, with straight sides conducive to stabilization.

5. Comparison with natural examples

The natural equivalent of a rigid particle with a surrounding weak layer is a mantled porphyroclast (Fig. 12), where a rigid mineral core is surrounded by a fine grained recrystallized aggregate extending into the foliation to form elongate tails (e.g. Passchier and Simpson, 1986; Passchier and Trouw, 1996, Section 5.6.5). Such tails or wings around a porphyroclast can develop from either a passive (Passchier and Simpson, 1986; Mandal et al., 2000) or a weaker mantle (i.e. weaker than the matrix, as in the present study). In natural mylonites, the development of thin elongate tails (Fig. 12c–f), similar to our experiments, is common. If the mantle is indeed weaker than the matrix, the present study shows that the rotational behaviour of the porphyroclast will be markedly altered and that the behaviour will depend on the mantle thickness (and therefore the recrystallization rate relative to the strain rate), the particle aspect ratio and shape. In nature, a thick mantle may be maintained around the porphyroclast by continuous recrystallization during deformation. This effect could not be realistically modelled in the analogue experiments. Intuitively, a steady-state mantle thickness along the long particle side, where tractions are most important for determining the rotational behaviour when the particle long axis is at a low angle to the shear direction, should tend to stabilize the particle. When productivity balances mantle thinning, a true stable end orientation for elongate elliptical particles may be possible (Schmid, 2002). However, in the experiments the thickness of the weak mantle could not be kept constant, with the result that the overall rotation rate decreased with increasing strain and consequent thinning of the weak mantle. This may not be unrealistic. In natural mantled porphyroclast examples, the recrystallization rate may also decrease rapidly as deformation increases. Recrystallization rate is high during initial stages of porphyroclast deformation at sites of stress concentration, such as asperities and irregularities, but slows down as grain refinement processes produce smooth elliptical to circular equilibrium shapes (ten Brink and Passchier, 1995). Therefore an evolution from a thick to a thin recrystallization mantle, as observed in the present experiments, is probably common in porphyroclasts. As a consequence, porphyroclasts that have acquired a strain-induced elliptical shape (Fig. 12f; Pennacchioni et al., 2001) may rotate slower than the Jeffery theory predicts. The significant increase in the differential rotation velocity (i.e. the difference between the maximum and minimum rotation rates during a complete rotation) and the decrease in the rotation rate compared with theory for angles α close to 0°, as observed in the experiments, would result in a very strong SPO subparallel to the shear plane for a population of elliptical porphyroclasts, as is indeed observed in some mylonites (Fig. 12b; Pennacchioni et al., 2001; Mancktelow et al., 2002).

For particles with a monoclinic shape, which is the case for most porphyroclasts with aspect ratio above three in Pennacchioni et al. (2001) (Fig. 12b–e) and Mancktelow et al. (2002), the SPO is more consistent with a stable end orientation with the long axis (enveloping ellipse) at a small antithetic angle to the shear plane. In accordance with the results of Mancktelow et al. (2002), the present experiments confirm that slip at the particle/matrix interface of a rhombohedral/monoclinic shaped particle can induce stabilization of a rigid particle in non-coaxial flow, with an orientation similar to that observed in natural examples (compare Fig. 12a and b). Mica-fish also commonly display a thin mantle of fine recrystallized or abraded material surrounding a single mica core (Fig. 12e), which could also act as a lubricating layer and explain their stabilization.

In the analogue experiments, the weak mantle layer is introduced around the rigid particle to produce detachment between particle and matrix, given the sticky character of PDMS. As discussed above, slip at the particle/matrix interface may indeed be due to the presence of a weak mantle of finely recrystallized material developed around many natural porphyroclasts. However, it could also develop by discrete failure at the interface if the traction exerted by the flowing matrix on the surface of an inclusion was sufficient to reach the yield surface. This depends on the physical properties of the matrix and particle surface, and in particular the local pore fluid pressure. Mandal et al. (2001) have shown theoretically that the stress state along the surface of an elliptical particle varies as a function of the particle aspect ratio and orientation and, therefore, that failure of the matrix/particle interface may occur for critical combinations of these parameters. In the Mont Mary and Finero mylonites (Pennacchioni et al., 2001; Mancktelow et al., 2002), porphyroclasts of elliptical to monoclinic shape do not show any evident mantles but the consistency of their SPO (Fig. 12b) with the particle kinematics observed in the rock-analogue experiments suggests that slip at the particle/matrix interface did occur during deformation. This results in an ‘anomalous’ behaviour compared with the commonly assumed Jeffery-type behaviour, but consistent with the behaviour of lubricated particles.

6. Conclusions

The new series of analogue experiments extends the work of Mancktelow et al. (2002), systematically investigating the influence of particle shape and the presence and thickness of a surrounding weak mantle layer on the behaviour of a rigid particle embedded in a linear viscous matrix undergoing simple shear. The different factors were independently studied to establish the influence of each parameter on the rotational behaviour of a rigid particle. This study confirms that the presence of a weak layer surrounding the particle has a strong influence on its rotational behaviour. In particular, it induces initial back

rotation, irrespective of the shape, when the long axis is initially nearly parallel to the shear plane. For all other initial positions considered in this study (i.e. ca. −30°, −60° and −90°) and irrespective of the aspect ratio, only synthetic rotation occurs. Whereas rhomboidal particles develop a stable orientation with the straight sides nearly parallel to the shear plane, elliptical particles with lubricated boundaries never reach a truly stable position. However, for more elongate particles the rotation rate when the long axis is sub-parallel to the shear plane is so slow that the orientation is quasi-stable for long periods. The influence of the thickness of the lubricating layer is explicitly considered for the first time in the current experiments and it has been observed that:

1. In all experiments in which the weak layer exceeded 10% in volume of the particle, irrespective of the aspect ratio, the particles rotate faster than the Jeffery theory predicts.
2. When the weak material is less than 10%, the particles tend to rotate slower than in the examples with a thicker soap layer. The less elongate particles (i.e. aspect ratio 2) show a rotational behaviour similar to theory, but more elongate particles (aspect ratios 3 and 6) rotate even more slowly and indeed slower than predicted by the Jeffery theory. At least for a Newtonian viscous matrix, the presence of planar weak layers in the adjacent matrix (without lubrication of the particle boundary) does not induce back rotation of an elliptical particle and indeed does not strongly affect the rotational behaviour. For this reason, it is unlikely that the elongate tails developed during ongoing shear have much direct influence on the rotational behaviour. Much more important is the lubrication of the long sides of the particles where tractions are most important in determining rotational behaviour, especially when the particle long axis is near parallel to the shear plane (i.e. in an orientation favourable for stabilization). These analogue results therefore provide a justification for the assumption in the complementary numerical modelling study of Schmid (2002) that the high strain geometry with elongate tails is not critical in evaluating the overall behaviour and that the system behaviour can be adequately considered in terms of two concentric cylindrical ellipses (near-rigid core and weak mantle, respectively).

In view of the similarities between porphyroclasts showing a very strong SPO (suggestive of a stable end-orientation) in real rocks and the results of the experiments, we infer the presence of a lubricating weak layer or discrete slip at the particle/matrix interface of these natural porphyroclasts. This factor combined with the shape of the porphyroclast could allow such rigid particles to attain a stable orientation. In particular, we suggest that slip could be induced by the layer of newly recrystallised (or abraded) grains often observed surrounding porphyroclasts. The elongation of this fine material into the matrix as thin tails, similar to the experiments, suggests that this fine mantle material is weaker than the surrounding matrix. The importance of the thickness of the weak layer in determining the rotational behaviour of rigid particles is clearly established in the current experiments. It follows that in natural mylonites the rotational behaviour of porphyroclasts may be strongly influenced by the relation between the recrystallization rate of a porphyroclast and the rate at which this finer-grained recrystallized material is removed or thinned by ongoing deformation.

Acknowledgements

The authors thank Yuri Podladchikov and Dani Schmid for fruitful discussions. Robert Hofmann constructed and maintained the ring-shear rig. Urs Gerber provided much welcome help in obtaining good quality digital photographs. Reviews by Saskia ten Grotenhuis and Tim Bell are gratefully acknowledged. Stefano Ceriani was funded by the "Universita' di Padova" in the frame of the "Progetto di di ricerca di Ateneo 1999: Le zone di shear milonitico: uno strumento di interpretazione reologica" and this funding is also gratefully acknowledged.

References

Arbaret, L., Mancktelow, N.S., Burg, J.-P., 2001. Effect of shape and orientation on rigid particle rotation and matrix deformation in simple shear flow. Journal of Structural Geology 23, 113–125.

ten Brink, C.E., Passchier, C.W., 1995. Modelling of mantled porphyroclasts using non-Newtonian rock analogue materials. Journal of Structural Geology 17, 131–146.

Dixon, J.M., Summers, J.M., 1985. Recent developments in centrifuge modelling of tectonic processes: equipment, model construction techniques and rheology of model materials. Journal of Structural Geology 7, 83–102.

Ferguson, C.C., 1979. Rotations of elongate rigid particles in slow non-Newtonian flows. Tectonophysics 60, 247–262.

Fernandez, A., Feybesse, J.-L., Mezure, J.-F., 1983. Theoretical and experimental study of fabrics developed by different shaped markers in two-dimensional simple shear. Bulletin de la Société géologique de France 7 (XXV), 319–326.

Freeman, B., 1985. The motion of rigid ellipsoidal particles in slow flows. Tectonophysics 113, 163–183.

Ghosh, S.K., Ramberg, H., 1976. Reorientation of inclusions by combination of pure shear and simple shear. Tectonophysics 34, 1–70.

ten Grotenhuis, S.M., Passchier, C.W., Bons, P.D., 2002a. The influence of strain localization on the rotation behaviour of rigid objects in experimental shear zones. Journal of Structural Geology 24, 485–499.

ten Grotenhuis, S.M., Piazolo, S., Pakula, T., Passchier, C.W., Bons, P.D., 2002b. Are polymers suitable rock analogs? Tectonophysics 350, 35–47.

Hinch, E.J., Leal, L.G., 1979. Rotation of small non-axisymmetric particles in a simple shear flow. Journal of Fluid Mechanics 92, 591–608.

Ildefonse, B., Mancktelow, N.S., 1993. Deformation around rigid particles: the influence of slip at the particle/matrix interface. Tectonophysics 221, 345–359.

Jeffery, G.B., 1922. The motion of ellipsoidal particles immersed in a viscous fluid. Proceedings of the Royal Society A102, London, 161–179.

Ježek, J., 1994. Software for modelling the motion of rigid triaxial ellipsoid particles in viscous flow. Computers and Geosciences 20, 409–424.

Ježek, J., Melka, R., Schulmann, K., Venera, Z., 1994. The behaviour of rigid triaxial particles in viscous flows—modelling of fabric evolution in a multiparticle system. Tectonophysics 229, 165–180.

Lister, G.S., Snoke, A.W., 1984. S–C mylonites. Journal of Structural Geology 6, 617–638.

Mancktelow, N.S., Arbaret, L., Pennacchioni, G., 2002. Experimental observations on the effect of interface slip on rotation and stabilisation of rigid particle in simple shear and a comparison with natural mylonites. Journal of Structural Geology 24, 567–586.

Mandal, N., Samanta, S.K., Chakraborty, C., 2000. Progressive development of mantle structures around elongate porphyroclasts: insights from numerical models. Journal of Structural Geology 22, 993–1008.

Mandal, N., Chakraborty, C., Samanta, S.K., 2001. Controls on the failure mode of brittle inclusions hosted in a ductile matrix. Journal of Structural Geology 23, 51–66.

Marques, F.O., Coelho, S., 2001. Rotation of rigid elliptical cylinders in viscous simple shear flow: analogue experiments. Journal of Structural Geology 23, 609–617.

Masuda, T., Mizuno, N., Kobayashi, M., Ngoc Nam, T., Otoh, S., 1995. Stress and strain estimates for Newtonian and non-Newtonian materials in a rotational shear zone. Journal of Structural Geology 17, 451–454.

Passchier, C.W., 1987. Stable positions of rigid objects in non-coaxial flow—a study in vorticity analysis. Journal of Structural Geology 9, 679–690.

Passchier, C.W., Simpson, C., 1986. Porphyroclast systems as kinematic indicators. Journal of Structural Geology 8, 831–843.

Passchier, C.W., Trouw, R.A.J., 1996. Microtectonics, Springer, Berlin, 289pp.

Pennacchioni, G., Di Toro, G., Mancktelow, N.S., 2001. Strain-insensitive preferred orientation of porphyroclasts in Mont Mary mylonites. Journal of Structural Geology 23, 1281–1298.

Reiner, M., 1969. Deformation, Strain and Flow, 3rd ed, H.K. Lewis & Co, London, 347pp.

Schmid, D., 2002. Finite and infinite heterogeneities under pure and simple shear. Ph.D. thesis, ETH Zürich.

Simpson, C., Schmid, S.M., 1983. An evaluation of criteria to deduce the sense of movement in sheared rocks. Geological Society of America Bulletin 94, 1281–1288.

Stewart, L.K., 1997. Experimental investigation of the effects of fluid heterogeneity upon the motion of rigid ellipsoidal inclusions during bulk inhomogeneous shortening. Journal of Structural Geology 19, 1231–1243.

Taylor, G.I., 1934. The formation of emulsions in definable fields of flow. Proceedings of the Royal Society A146, 501–523.

Weijermars, R., 1986. Flow behaviour and physical chemistry of bouncing putties and related polymers in view of tectonic laboratory applications. Tectonophysics 124, 325–358.

Willis, D.G., 1977. A kinematic model of preferred orientation. Geological Society of America Bulletin 88, 883–894.